VISUALLY CONTROLLED HELICOPTER: A CONTROL SCHEME FOR HELICOPTER LANDING

Quang Huy Truong*
quang_huy.truong@onera.fr
ONERA / DCSD
Salon de Provence, BA 701, 13661
France
(*) PhD student

Thomas Rakotomamonjy
thomas.rakotomamonjy@onera.fr
ONERA / DCSD
Salon de Provence, BA 701
France

Jean-Marc Biannic
jean-marc.biannic@onera.fr
ONERA / DCSD
Toulouse, 2 avenue Edouard Belin,
BP 74025, 31055 France

Abstract

This paper introduces a system combining visual servoing and Translational Rate Command (TRC), an advanced control law for modern helicopters. This controller is used to follow a ship and land on its helideck. A method based on a simplified and uncoupled model to tune the controller is presented as well. In this first approach the landing procedure is set as fully automatic, but as the final goal is to provide the pilots with an assistance based on these controllers, an eye is kept on flying and handling qualities of the closed loop helicopter. Therefore controllers are tested in order to assess stability and good flying characteristics. Models include helicopter and ship dynamics, nonlinear actuators, and aircraft-embedded camera.

NOMENCLATURE

$\delta_{col}, \delta_{lat}, \delta_{lon}, \delta_{ped}$	Primary helicopter inputs (collective, lateral cyclic, longitudinal cyclic and pedal)
u, v, w	Helicopter ground velocity, given in body frame.
p, q, r	Body-axis angular rates
Φ, θ, ψ	Euler angles giving aircraft orientation relative to the Earth
x, y, z	Position in Earth frame (North-East-Down coordinates)

MAIN ACRONYMS

AC	Attitude Control
ACAH	Attitude Command Attitude Hold
DOF	Degree(s) of Freedom
IBVS	Image-Based Visual Servoing
MTE	Mission Task Element
PID	Proportional Integral Derivative
TRC	Translational Rate Command
UAV	Unmanned Air Vehicle

1. INTRODUCTION

1.1. Context of the research

Landing a helicopter is a very difficult task due to numerous phenomena that naturally threaten pilot control. For offshore landing (on ship or platform) it is particularly complex because of an unusual and stressful environment for the pilot: a singular wind (ship air wake), weather not often accommodating, and even a moving deck in the case of ship landing [1][2]. Aid systems exist to help pilots during that procedure, such as visual indicators, helicopter stabilising systems (ex: Stability Augmentation System) or the ship crew. However pilots still have to deal with a lot of work to land safely.

In this context, ONERA (The French Aerospace Lab) is aiming to provide tools to help pilots more, using models and simulators installed in their engineering flight simulator facility called *PycsHel – Prototype and Design of Helicopter Systems*, in the Department of Systems Controls and Flight Dynamics (DCSD) at ONERA Salon-de-Provence.

1.2. Techniques for ship landing – Choice for visual servoing

Many techniques can be found to follow a ship landing procedure in the literature. For instance, some are based on using a tether to guide the autonomous landing [3], some on predictions of ship deck movements [4] to detect calm opportunities [5] or to measure data for an automatic landing [6], and some are based on visual information. Recent developments on embedded systems allowed controllers to use always more powerful algorithms to provide methods for piloting, guidance and navigation based on visual information, sometimes instead of inertial or cinematic data. Nowadays these techniques are common to control UAVs automatically.

1.3. Visual servoing – Applications

The basic idea with visual servoing is to use data from camera images to generate a command to displace the camera. Two approaches can be considered: Image-Based Visual Servoing (IBVS) or Position-Based Visual Servoing (PBVS) [7]. In both cases, a desired velocity to be tracked by the camera is generated, but IBVS uses directly image

features given by the image while PBVS first estimate the 3D target pose compared to the camera. The pose estimation can also be useful to get new measurements, for instance to estimate height between camera and the ground [8], or to predict movements of a platform to land on it [9][10]. The approach of this paper focuses on IBVS technique as it is more robust to noise and coarse estimations, and can be used with a camera alone, as explained in [7]. Literature for visually controlled UAVs provides many applications where IBVS is combined with inertial measurements [11] or GPS [12]. In [13] this combination is particularly interesting as it combines IBVS and a Translational Rate Command (TRC) law, based on Proportional Derivative (PD) controllers, with an inner Attitude Control (AC) loop. This architecture can be found among existing helicopter control schemes. Therefore visual servoing can be beneficial to provide a good landing system, first automatically but also to the pilot for manual control.

1.4. Flying/Handling qualities for ship landing

Ship landing depends on so many factors that the common standard for rotorcrafts, the ADS-33E-PRF [14], does not include this case. As a result flying and handling qualities for ship landing cannot be summed up in one MTE despite several studies about that issue [15]. However analogies can be made under conditions, for instance a procedure with a calm sea can be seen as a Hover and Landing MTEs. Then criteria used in this paper to define the flying qualities followed by the closed-loop system will be based on the existing Hover and Landing MTEs.

1.5. Objectives

This paper presents a method to set a simple controller based on a TRC law and IBVS. The main goal is to follow a ship and land on it, using image features as references while filtering its movements to get a smooth and realistic helicopter trajectory compared to the targeted ship. The global TRC architecture is defined by:
- An inner AC control loop
- An outer velocity control loop (called AC-TRC in this paper)

These controllers are built based on standard Proportional Integral Derivative (PID) architectures. This architecture is suggested by the handling qualities requirements for TRC systems given in [16]. AC and TRC are usually set to be directly commanded by the pilot's control sticks – then controls are known as ACAH (Attitude Command, Attitude Hold) in standards. Each law has an influence on one specific order dynamics, which means the effect is a trade-off between being slow and stable or fast and easily unstable. The choice

between ACAH and TRC depends on the needed response-type according to the studied case. As the latter cannot be defined with predefined MTEs, TRC and ACAH systems are considered as options for the pilot, therefore gains are tuned for each law according to usual response-type criteria.

The closed-loop system is set as automatic, but the final purpose is to provide optimal commands to be followed by pilots for ship tracking and landing, as part of a research project led at ONERA. Tools are given to tune the controllers based on required flying and handling qualities.

2. SIMULATION ENVIRONMENT

2.1. *The closed-loop system*
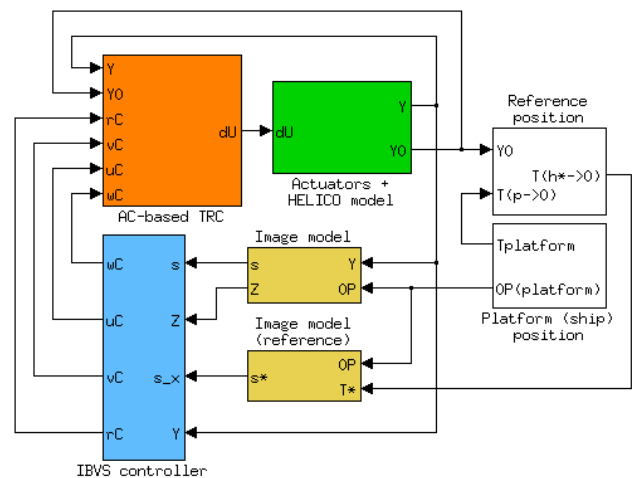
Figure 1 – General Architecture

The global architecture presented above represents an 11-ton cargo-type helicopter model with nonlinear actuators (green), the TRC (orange) and IBVS (blue) controllers, and the cameras converting absolute positions into camera images (current and reference positions), and representing the targets into image features (yellow). Ship and reference positions (white) are used as primary inputs for the desired trajectory.

2.2. Models and assumptions

Two helicopter models were used in this paper: a nonlinear model for simulation results, and its linearization around an equilibrium state X_E for analytical studies and gain tuning. In both cases, the notation used is clarified in Table 1.

Variable	Notation
δU	$[\delta_{col}\ \delta_{lat}\ \delta_{lon}\ \delta_{ped}]^T$
δX	$[\delta u\ \delta v\ \delta w\ \delta p\ \delta q\ \delta r\ \delta \Phi\ \delta \theta\ \delta \psi]^T$

Table 1. Control inputs *δU* and state vector *δX*

Helicopter dynamics was linearized around X_E to get a state space system $\delta \dot{X} = A\delta X + B\delta U,$ a detailed

description can be found in [17]. The equilibrium state X_E is chosen in order to start with a specific desired translational speed (here this is the average horizontal speed of the ship). Measurements Y include the state $X = \delta X + X_E$ and its derivatives, without noise. It is assumed that at time t = 0 the state is at equilibrium, therefore the initial state (through the initial measurements Y_0) is also recorded. The nonlinear model is the HOST[1] code that simulates a realistic heavy helicopter with nonlinear aeromechanical dynamics.

The actuators take into account delay (around 10ms, approximated by a first-order filter), natural actuator dynamics (through a third-order transfer function) with position saturation. Ship helideck displacements were modelled along the x, y, Φ and θ axes, from data given in [6] to be close to a moderate sea (see state 4).

Assumption: The automatic procedure starts from an initial equilibrium condition, at a speed close to the ship horizontal speed, and at a distance to the ship small enough so that the helicopter camera can see the ship helideck from above. That camera is positioned high at the front of the rotorcraft, pointing directly under the aircraft along its Z axis, so that most of the ground points can be captured once landed.

2.3. TRC controller
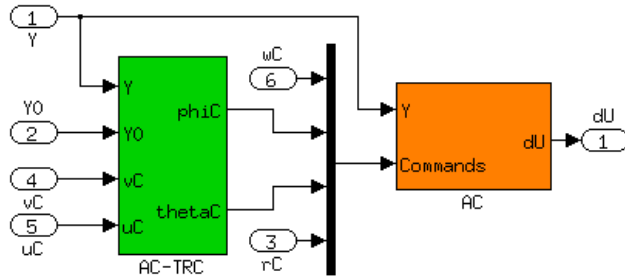
Figure 2 – TRC subsystem structure

As introduced earlier, this TRC includes an inner AC loop and an outer AC-TRC loop, as shown in Figure 2, both based on PID controllers.

Law	Inputs					Outputs
AC	Measurements	w	$\delta\phi, p$	$\delta\theta, q$	r	$\delta_{col}, \delta_{lat},$
	Commands	w^c	$\delta\phi^c$	$\delta\theta^c$	r^c	$\delta_{lon}, \delta_{ped}$
AC-TRC	Measurements	u		v		$\delta\phi^c, \delta\theta^c$
	Commands	u^c		v^c		

Table 2. Inputs/Outputs of AC and AC-TRC controllers

PID gains are easily embeddable and certifiable, and can be tuned to reduce cross couplings that

---

[1] Helicopter Overall Simulation Tool © developed by Airbus Helicopter, ONERA, DLR [18]

naturally exist with helicopters. A tuning procedure can be found in [19] where a method is detailed to design decoupling PID controllers for an AC law while accounting for handling and flying qualities. Inputs/Outputs of the AC and AC-TRC controllers are presented in Table 2.

Helicopters are underactuated machines with only four control inputs. As a result the AC inner loop is designed to use only four inputs and lead to equilibrium states. Then, even though the IBVS law generates a 6-DOF velocity command [7], the TRC controller can use only four commands out of six from the IBVS. AC control laws are described by equations (1) while AC-TRC laws correspond to equations (2). Gains are calculated as presented in section 3.

$$(1) \quad \begin{cases} \delta_{col} = K_{dw}\dot{w} + K_w(w - w^C) + K_{iw}\int w - w^C \\ \delta_{lat} = K_p p + K_\phi(\delta\phi - \delta\phi^C) + K_{i\phi}\int \delta\phi - \delta\phi^C \\ \delta_{lon} = K_q q + K_\theta(\delta\theta - \delta\theta^C) + K_{i\theta}\int \delta\theta - \delta\theta^C \\ \delta_{ped} = K_{dr}\dot{r} + K_r(r - r^C) + K_{ir}\int r - r^C \end{cases}$$

$$(2) \quad \begin{cases} \delta\phi^C = K_{dv}\dot{v} + K_v(v - v^C) + K_{iv}\int v - v^C \\ \delta\theta^C = K_{du}\dot{u} + K_u(u - u^C) + K_{iu}\int u - u^C \end{cases}$$

2.4. Camera model
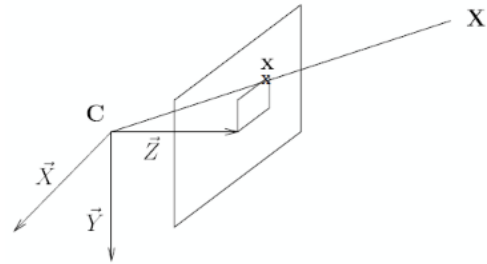
Figure 3 – Projection of a target point onto the image frame

The main variables used for visual servoing are the image features s, here image-plane coordinates of the helideck points directly measured from the image, as presented in (3), and calculated after projections on the image frame, as seen in Figure 3.

$$(3) \quad s = \begin{bmatrix} x \\ y \end{bmatrix} = \begin{bmatrix} X/Z \\ Y/Z \end{bmatrix} = \begin{bmatrix} u - c_v/f\alpha \\ v - c_v/f \end{bmatrix}$$

Projections use the target point coordinates (X, Y, Z) in the camera frame (centred in C). The feature s is calculated in real time, given the points coordinates (u, v) measured in the current image, in pixels, and the camera intrinsic parameters that are:
-    The central point coordinates (c_u, c_v) in pixels,
-    The focal length f,
-    The ratio in pixel dimensions α.

Distances Z between targeted points and camera

frame are also assumed measured for IBVS control.

2.5. IBVS controller – Principles

The IBVS introduced in this section is based on a standard geometric approach detailed in [7] and [20]. From (3) is deduced the relation (4) between a visual feature s_i and the camera velocity v_c, using an interaction matrix L_i related to s_i.

$$(4) \qquad \dot{s}_i = L_{s_i}(s_i)v_c + \frac{\partial s_i}{\partial t}$$

$$(5) \quad L_i = \begin{bmatrix} -1/Z_i & 0 & x_i/Z_i & x_iy_i & -(1+x_i^2) & y_i \\ 0 & -1/Z_i & y_i/Z_i & 1+y_i^2 & -x_iy_i & -x_i \end{bmatrix}$$

The second term of (4) represents the time variation of the image feature s_i due to the usually unknown target motion (here a point on the ship helideck).

Visual servoing is based on an error $e = s - s^*$ to minimise, s^* being a reference image feature to follow.
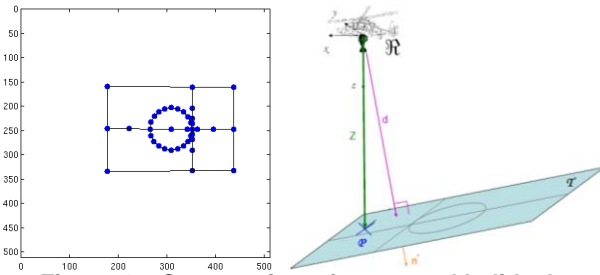
Figure 4 – Camera view of a targeted helideck

For IBVS applications s is defined by several points $s_i = [x_i \quad y_i]^T$ coordinates from the targeted helideck. Hence the target (helideck) is identified as presented in Figure 4. Consequently the final error can be summed up in (8).

$$(6) \qquad s = [s_1^T \quad s_2^T \quad ...]^T$$

$$(7) \qquad L_e = L_s = \begin{bmatrix} L_1 \\ L_2 \\ ... \end{bmatrix}$$

$$(8) \qquad \dot{e} = L_e v_c + \frac{\partial e}{\partial t}$$

Based on this structure of (8) a distinction is found between two specific sources of errors.

- The camera displacement: $L_e v_c$
- The target displacement: $\dfrac{\partial e}{\partial t}$

The chosen approach to reduce the error is to define a command in velocity. This command was provided in [20] and takes into account both sources of errors. The matrix L_e^+ is the Moore-Penrose pseudo-inverse

of the interaction matrix L_e, and λ is the IBVS gain.

$$(9) \qquad v_c = -\lambda L_e^+ e - L_e^+ \frac{\widehat{\partial e}}{\partial t}$$

$$(10) \qquad L_e^+ = (L_e^T L_e)^{-1} L_e^T$$

$$(11) \qquad \dot{e} = -\lambda L_e L_e^+ e$$

The differential equation (11) finally defines the problem to be solved. The whole algorithm has been simulated using a visual servoing toolbox (http://vstoolbox.sourceforge.net).

3. GAIN TUNING

This section introduces a method to get a first set of gains for each controller.

3.1. IBVS controller

The previous section shows the IBVS law mainly depends on the geometry between target points and embedded camera. The controller is independent of the system dynamics. In terms of stability the interaction matrix L_e should be full rank to control the 6 DOF, which is possible with a minimum of 3 points in the image. However, in some configurations L_e can be singular with less than 4 points as explained by Chaumette in [7]. This situation is not desired to get the pseudo-inverse L_e^+. As a result a minimum of 4 points is a necessary condition.

Another stability condition is related to the proportional gain λ. Setting this gain to a positive value is sufficient to ensure stability of the IBVS controller. It can be chosen high for fast system responses but not too high due to the helicopter dynamical limits. This choice is justified by the TRC sensibility: with high variations in velocity commands the TRC controller would need a high attitude command, which can saturate the actuators and create instabilities. Therefore λ is not set too high to provide realistic commands.

The last stability condition is to get the best estimate of the term related to the target displacement. An estimate (12) can be calculated thanks to (8) then used in the control law. The objective is to get (13) to cancel its influence in (8). In the process the camera velocity is measured, the image error as well. To avoid instabilities created by steps in the reference image feature s^*, the time variation of the error is approximated as (14).

$$(12) \qquad \frac{\widehat{\partial e}}{\partial t} = \hat{\dot{e}} - L_e \hat{v}_c$$

(13)
$$L_e L_e^+ \frac{\widehat{\partial e}}{\partial t} \approx \frac{\partial e}{\partial t}$$

(14)
$$\hat{e} \approx \dot{s}$$

3.2. TRC controller

The approach used here was introduced by Antonioli in [19] to set gains for an AC law. This method is rewritten to also tune the AC-TRC controller. The purpose of this approach is to decouple the different laws, each one of them was designed for specific purposes and focus only on one axis, not the others. As a result the closed loop system is approximated as a simplified one-axis closed loop system, and only one control law is studied at a time, other control laws are set null. In addition some model approximations are used to ease gain tuning:

- Actuators are modelled with a transfer function $A(s) = A_n(s)/A_d(s)$ in Laplace space, and included before each component of δU. In time space the effect is written as $A(\delta_{lat})$
- Pure lateral/longitudinal flight: $p \approx \delta\dot{\phi}$ and $q \approx \delta\dot{\theta}$, and cross couplings between states are assumed cancelled. This approximation is also justified in [17].

Therefore, for a pure lateral flight, calculations give the simplified system (15). Parameters $(L_p, L_\phi \dots)$ come from the linearized state space system $\delta\dot{X} = A\delta X + B\delta U$.

(15)
$$\begin{cases} \dot{p} \approx L_p p + L_\phi \delta\phi + L_{\delta lat} A(\delta_{lat}) \\ \dot{v} \approx Y_v v + Y_\phi \delta\phi + Y_{\delta lat} A(\delta_{lat}) \end{cases}$$

From the simplified model (15) the following equations were deduced in the Laplace space, with parameters expressed in (19). The AC transfer function (18) is deduced directly from the Laplace form of (16) and (1). This transfer function $\delta\phi/\delta\phi^c$ is called $G_A(s)$ in the next equations.

(16)
$$A(\delta_{lat}) = \frac{\dot{p} - L_p p - L_\phi \delta\phi}{L_{\delta lat}}$$

(17)
$$\frac{v}{\delta\phi} = s\frac{Y_0 + Y_1 s + Y_2 s^2}{s - Y_v} = H_{v\phi}(s)$$

(18)
$$\frac{\delta\phi}{\delta\phi^c} = \frac{(L_{\delta l1}s + L_{\delta l2})A(s)}{s^3 + \widehat{L_p}(s)s^2 + (L_{\delta l1}s + L_{\delta l2})A(s)}$$

(19)
$$\begin{cases} \widehat{L_p}(s) = -(L_p + L_{\delta lat}A(s)K_p) \\ L_{\delta l1} = -L_{\delta lat}K_\phi \\ L_{\delta l2} = -L_{\delta lat}K_{i\phi} \end{cases}$$

The expression (17) is first deduced using (15) and (16). Then the control law (2) is rewritten as (20). Finally (17), (18) and (20) are combined to get the AC-TRC transfer function (21).

(20)
$$\begin{cases} \delta\phi^c = K_T(s)v - K_T'(s)v^c \\ K_T' = \frac{K_{iv}}{s} + K_v \\ K_T = K_T' + K_{dv}s \end{cases}$$

(21)
$$\frac{v}{v^c} = \frac{K_T'(s)G_A(s)H_{v\phi}(s)}{K_T(s)H_{v\phi}(s)G_A(s) - 1}$$

(22)
$$\begin{cases} Y_0 = Y_\phi - L_\phi Y_{\delta lat}/L_{\delta lat} \\ Y_1 = -L_p Y_{\delta lat}/L_{\delta lat} \\ Y_2 = Y_{\delta lat}/L_{\delta lat} \end{cases}$$

The transfer functions (18) and (21) are interesting to set the AC and AC-TRC gains, as they can be studied to tune the PIDs. Therefore it initialises a first set of gains. Classical control synthesis tools such as Routh-Hurwitz or Nyquist criteria can be valuable for a start, but the following section is more useful to get a controller ready for ship landing.

3.3. Linear model analysis

The last transfer functions needed for a simplified model are summed up below, with parameters written in (26)-(27). They are all deduced from simplified state space systems written in a form similar to (15), as presented in (23). The term N_ψ is equal to zero then not written in (23).

(23)
$$\begin{cases} \dot{w} \approx Z_w w + Z_{\delta col}A(\delta_{col}) \\ \dot{r} \approx N_r r + L_{\delta ped}A(\delta_{ped}) \end{cases}$$

(24)
$$\frac{w}{w^c} = \frac{(Z_{\delta l1}s + Z_{\delta l2})A(s)}{Z_0(s)s^2 + Z_w s + (Z_{\delta l1}s + Z_{\delta l2})A(s)}$$

(25)
$$\frac{r}{r^c} = \frac{(N_{\delta l1}s + N_{\delta l2})A(s)}{N_0(s)s^2 + N_r s + (N_{\delta l1}s + N_{\delta l2})A(s)}$$

(26)
$$\begin{cases} Z_0(s) = Z_{\delta col}K_{dw}A(s) - 1 \\ Z_{\delta l1} = Z_{\delta col}K_w \\ Z_{\delta l2} = Z_{\delta col}K_{iw} \end{cases}$$

(27)
$$\begin{cases} N_0(s) = N_{\delta ped}K_{dr}A(s) - 1 \\ N_{\delta l1} = N_{\delta ped}K_r \\ N_{\delta l2} = N_{\delta ped}K_{ir} \end{cases}$$

From these functions poles diagrams are sketched and compared to the poles of the actual linear systems used to model a helicopter.
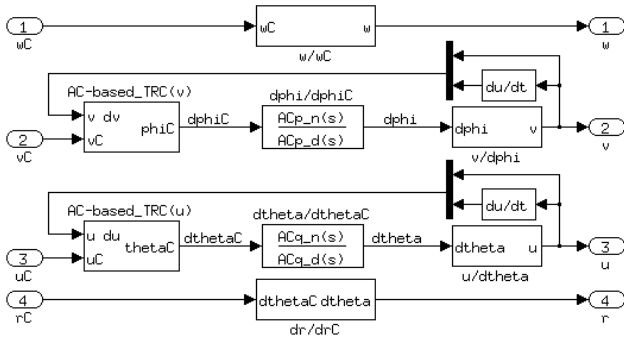
Figure 5 – Simplified linear system

A quite easy way to study the simplified linear system was to simulate the whole system through a Simulink model that separately represents each axis with its functions, as seen in Figure 5. In the next figures poles are drawn with the limits on pitch and roll oscillations defined for Hover and Low Speed MTEs [14].
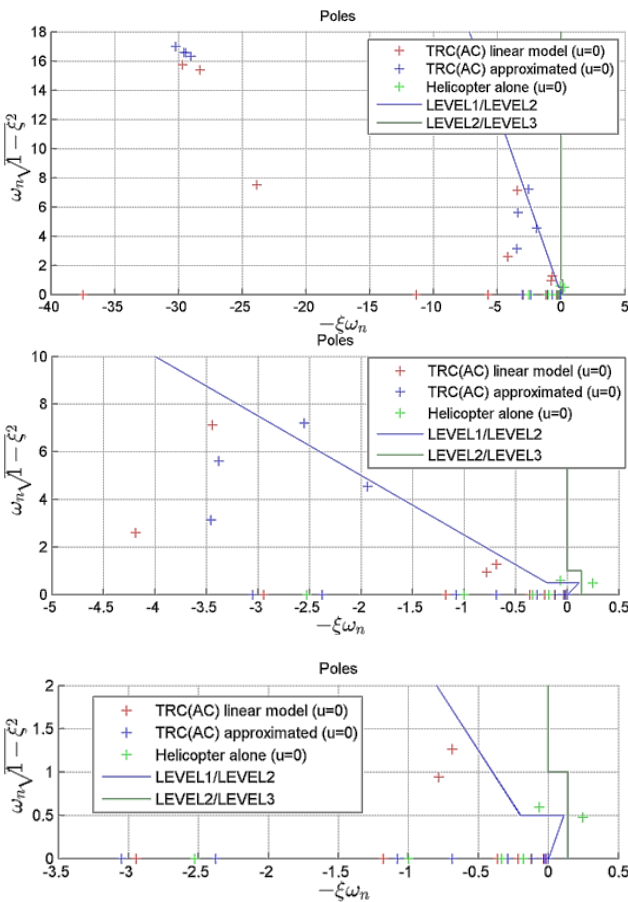
Figure 6 – Resulting poles for a Hover flight

The chosen set of gains respects well the LEVEL1 requirements, as seen in Figure 6. To assess the efficiency of the chosen gains it is also useful to evaluate the poles with different horizontal speed values: as the ship is actually moving the helicopter must follow it with a similar speed. Therefore a sweeping between models (for translational speeds from 0 kt. – hover – to 25 kt.) has been carried out

while sketching the poles in the pole diagram. As hoped the chosen set of gains follows well the expectations as shown in Figure 10 (see Appendix A).

Obviously the simplified helicopter model based on transfer functions is not exactly representative of the full linear one. However it is sufficient enough to provide good results in terms of pole placement. In addition, working with uncoupled laws helps to identify particular helicopter modes, as seen in Figure 10. This is helpful to set specific gains to get desired qualities.

4. SIMULATIONS

4.1. Procedure

As introduced by Lumsden [1], the proposed mission is to reach a point above the ship helideck, then to land on the ship. The chosen approach before landing is the Astern approach, usual in the French navy and presented in [21] and in Figure 7.
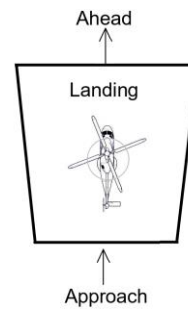
Figure 7 – Schematic representation of the Astern approach [21]

Aspect	Parameter	Conditions
Operational	Approach	Astern
	MTEs	Hover, Landing
Helicopter	Class	Cargo (11 tons)
	Initial position and orientation	Behind the ship, random position
	Initial velocity	Close to the ship average velocity
	Initial height	15 ft. (4.57 m) above helideck
Ship	Deck movements	Sea state 4
	Wind-Over-Deck	Intensity: 0 kt. Direction: 0° [2]
	Deck average height	17 ft. (5.18 m)
	Average horizontal velocity	20 kt.

Sea states are defined based on the Douglas Sea

---

[2] Relative wind direction: at 0° wind blows from the bow of the ship

Scale. Based on information given in [6] (see Appendix B for details), amplitudes and main frequencies used to model platform motion are deduced and shown in Table 3.

DOF	Amplitude (deg. or ft.)	Temporal pulsation ω (rad/s)	Wavelength λ (m)
Roll ϕ	3.8 deg.	0.803	/
Pitch θ	3.55 deg.	1.014	/
Yaw ψ	0.95 deg.	0.56	/
Heave z_p	4.92 ft. (1.5 m)	0.804	200

Table 3. Platform motion: Sea state 4

Platform heave was generated as an acoustic wave, such as $z_p(t) = z_p^A \sin\left(\omega t - \frac{2\pi}{\lambda} x_p(t)\right)$ where $x_p(t)$ is the helideck position through time.

Initial state: At the end of the approach, from behind the ship. To assess the quality of this automatic procedure, simulations were carried several times from different initial positions in (x,y) behind the ship at a longitudinal distance of 15 ft. max. This margin is justified as the camera must have an eye on the helipad. Otherwise the visual control is impossible. Helicopter's longitudinal and lateral axes are almost parallel to the deck's lines.

4.2. Expectations

As the MTE chosen for this procedure are Hover and Landing, few requirements are made in terms of performances. The desired expectations in accuracy are given in the Table below.

Desired performance	GVE	DVE
Maintain altitude of 15 ft. above helideck within	$\pm$2 ft.	$\pm$2 ft.
Maintain longitudinal/lateral position within	$\pm$3 ft.	$\pm$3 ft.
Maintain heading within	$\pm$5 deg.	$\pm$5 deg.
Attain a stabilised hover within	5 sec	10 sec

Table 4. Performance – Ship landing "hover"

Desired performance	GVE	DVE
Once altitude below 10 ft., complete the landing within	5 sec	5 sec
Longitudinal and lateral touchdown within	$\pm$3 ft.	$\pm$3 ft.
Attain a rotorcraft heading at touchdown aligned with the reference heading within	$\pm$10 deg.	$\pm$10 deg.

Table 5. Performance – Ship landing touchdown

Requirements for hover and landing performances are the "Adequate performances" from the true MTEs, which allows higher margins. Nevertheless

the relative altitude requirement (above helideck) for Hover may be too restrictive as the helideck is actually moving. The timing allowed for touchdown is based on actual ship landing requirements.

4.3. Results

Simulation results are shown in Appendix B. From these results it is noticeable that the global task is executed correctly.

4.3.1. Hover

It is especially the case for the Hover MTE. All initial states start from different positions behind the ship and all situations end up to the objective position above the ship with the desired performances, even though deck oscillations occur.

It takes between 5 and 10 seconds to reach the hover position (Figure 11), depending on the initial state. In (x, y, z) the desired pose is kept with an error less than 1.5 ft. vertically, laterally and longitudinally, whatever the initial position was compared to the ship. Heading is also kept within the limits, with oscillations limited under 2 degrees, as hoped (Figure 13).

4.3.2. Landing and touchdown

Results for landing and touchdown are similar, but not as obvious for a good touchdown.

Based on Figure 11 it takes 9.84 seconds from the moment when the altitude between helideck and helicopter is below 10 ft. to the first touchdown, which seems too long based on the expectations. However a local minimum in altitude is reached at t = 25 sec (after 3 sec) for a relative altitude of 1 ft. At that moment the actual vertical speed w is quasi null. In the scenario when pilot is still handling the command he can finish his landing at that moment.

Even with this, the accuracy remains good in both situations as shown in Figure 11 and Figure 13:
- Lateral/longitudinal position error under 1.5 ft.
- Heading error (helicopter heading compared to the helideck heading) under 2.5 degrees.

4.4. Limitations

As seen in Figure 15 saturations can occur with actuator commands. This is an undesirable side effect possible only when the initial position error is too high. In these examples, and nothing is currently implemented to neutralize this saturation effect.

Another point not considered yet is the measurement noise from both inertial sensors and camera, which can affect the accuracy. Minimum variance estimator (e.g. Kalman filtering) could be

used to address this case.

The last point not considered is the control limitations that should be added to always keep the target in the camera field of view. The current simulations suppose the target (helideck) is always on view, which is actually not necessarily the case.

5. HANDLING AND FLYING QUALITIES

Once controllers are tuned it is also interesting to assess the actual flying qualities of the system, based on the case studies/MTEs. Even though the ADS-33 is not relevant for this mission it is still possible to be inspired by the usual criterion defined in this standard. In addition this standard is defines qualities for piloted helicopters, not for fully automatic laws. However it is still interesting to consider working with these criteria if it is assumed that pilots follow exactly the commands provided by IBVS, TRC, or AC controllers. Therefore a required response-type can be set.

The following sub-sections remind the three main criterions of the standards: stability, agility (quickness) and accuracy (ability to follow fast inputs accurately). For each criterion the requirements are evaluated between LEVEL1 (good) and LEVEL3 (bad).

5.1. Stability criterion

The stability criterion is based on the eigenvalues placement. The basic idea is to sketch the main eigenvalues of the dynamic closed loop system and locate them to determine in which LEVELs they are to assess the flying qualities. The shape of the limits between LEVELs depends on the MTE, DOF and Response-type considered. In Figure 6, poles are studied for roll and pitch oscillations. Poles are all in the LEVEL1 area, which shows that the current gains can provide a good behaviour.

5.2. Agility criterion

The agility criterion is based on the time response after moderate changes. A quickness criterion is defined and takes into account peak in rates and changes.

In the example below, the agility criterion Q for an ACAH response-type is calculated after measuring the peak roll rate p_{pk} and the peak roll change $\Delta\phi_{pk}$ then Q is drawn in the associated diagram as a function of $\Delta\phi_{min}$.

$$(28) \qquad Q = \frac{p_{pk}}{\Delta\phi_{pk}} = f(\Delta\phi_{min})$$
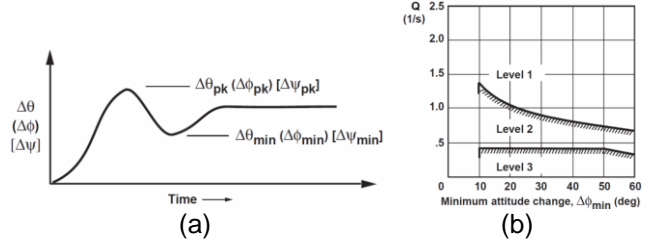
Figure 8 – Estimations of attitude quickness parameters during attitude change (a) and attitude quickness criterion (b), as presented in ADS-33 [14]

5.3. Accuracy criterion

The accuracy criterion is based on the frequency response after small changes. Main variables are extracted from the phase diagram of the studied responses.

$$(29) \qquad \tau_p = \frac{\Delta\phi_{2\omega_{180}}}{57.3(2\omega_{180})} = f(\omega_{BWphase})$$
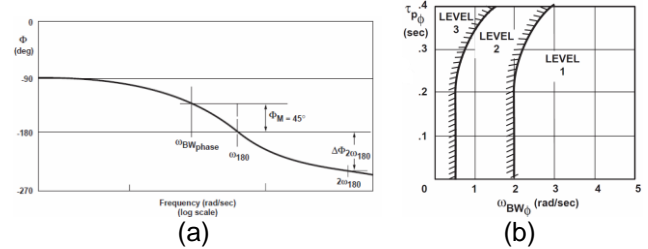
Figure 9 – Estimation of parameters (a) and accuracy criterion (b), as presented in ADS-33 [14]

In this example the accuracy criterion uses the cut-off bandwidth (ω_{180}), the bandwidth phase $(\omega_{BWphase})$ and the variation in phase $(\Delta\phi_{2\omega_{180}})$ to describe handling qualities of an ACAH law.

6. CONCLUSIONS

This paper presented a vision-based controller defined for an automatic ship landing. A full procedure to set gains and define expected stability quality is exposed with an actual process to assess the results between models. Evaluations obtained through different simulations led to encouraging perspectives for a potential use under calm and moderate seas (sea states 4 maximum). In terms of handling and flying qualities further studies would be necessary to assess agility and accuracy for ACAH and TRC response types, by first defining the adequate LEVEL limits.

7. FUTURE WORK

Further work will deal with the implementation of a feedforward controller in order to limit the risk of saturation by taking into account the model limits. This feedforward controller may be built as an anti-windup system whose design would be based on the full model used in this paper.

In parallel the control laws presented in this paper will also be implemented on the real time flight simulator *PycsHel* for flight tests with actual pilots.

8. REFERENCES

[1] Lumsden R B, Wilkinson C H and Padfield G. D. Challenges at the Helicopter-Ship Dynamic Interface, *24th European Rotorcraft Forum*, Marseille, France, Sept 1998.

[2] Taghizad A, Verbeke C, Desopper A. Aerodynamic perturbations encountered by a helicopter landing on a ship – Effects on the helicopter flight dynamics, *RTO AVT Symposium on "Fluid Dynamics Problems on Vehicles Operating near or in the Air-Sea Interface*", 1998.

[3] Oh S R, Pathak K, Agrawal S, Pota H, Garratt M. Approaches for a tether-guided landing of an autonomous helicopter. *IEEE Transactions on Robotics*, Vol. 22 (3), 536-544, 2006.

[4] Yang X, Pota H, Garratt M, Ugrinovskii V. Prediction of vertical motions for landing operations of UAVs. *47th IEEE Conference on Decision and Control*, 5048-5053, 2008.

[5] Fourie C, Jones T. Augmenting the helicopter-ship dynamic interface using an autonomous safe-landing prediction scheme. *International Conference on Unmanned Aircraft Systems*, 26-33, 2015.

[6] Horn J F, Yang J, He C, Lee, D. Autonomous ship approach and landing using Dynamic Inversion Control with Deck Motion Prediction. *41st European Rotorcraft Forum*, 2015.

[7] Chaumette F and Hutchinson S. Visual Servo Control, Part I: Basic approaches, *IEEE Robotics & Automation Magazine*, Vol. 13, pp. 82-90, 2006.

[8] Yu Z, Nonami K, Shin J, Celestino D. 3D vision based landing control of a small scale autonomous helicopter. *International Journal of Advanced Robotic Systems*, 4(1), 51-56, 2007.

[9] Hu B, Lu L, Mishra S. Fast, safe and precise landing of a quadrotor on an oscillating platform. *American Control Conference*, 3836-3841, 2015.

[10] Sanchez-Lopez J L, Pestana J, Saripalli S, Campoy P. An Approach Toward Visual Autonomous Ship Board Landing of a VTOL UAV. *Journal of Intelligent & Robotics Systems*, Vol. 74(1), 113-127, 2014.

[11] Herissé B, Hamel T, Mahony R, Russotto F-X. Landing a VTOL Unmanned Aerial Vehicle on a Moving Platform Using Optical Flow. *IEEE Transactions on Robotics*, Vol. 28(1), 77-89, 2011.

[12] Saripalli S, Montgomery J F, Sukhatme G S. Visually-Guided Landing of an Unmanned Aerial Vehicle. *IEEE Transactions on Robotics and Automation*, Vol. 19(3), 371-380, 2003.

[13] Ceren Z, Altug E. Vision-based servo control of a quadrotor air vehicle. *IEEE International Symposium on Computational Intelligence in Robotics and Automation*, 84-89, 2009.

[14] Baskett B J and Daniel D L O. Aeronautical Design Standard, Performance Specification, Handling Qualities Requirements for Military Rotorcraft, *US Army Aviation and Missile Command Std*, 2000.

[15] Padfield G D and Wilkinson C H. Handling Qualities Criteria for Maritime Helicopter Operations. *American Helicopter Society Forum 53*, 1997.

[16] Dudgeon G and Gribble J. Helicopter translational rate command using individual channel analysis and design, *UKACC International Conference on Control*, Vol. 1, No. 427, pp. 632-637, Sept 1996.

[17] Padfield G D. Helicopter Flight Dynamics: The Theory and Application of Flying Qualities and Simulation Modelling. Blackwell Publishing, Oxford, 2007.

[18] Benoit B, Dequin A-M, Kampa K, Grunhagen W, Basset P-M & Gimonet B. HOST, a general helicopter simulation tool for Germany and France, *56th Annual Forum of the American Helicopter Society*, 2000

[19] Antonioli J-C, Taghizad A, Rakotomamonjy T, Ouladsine M. Toward the development of a methodology for designing helicopter flight control laws by integrating handling qualities requirements. *40th European Rotorcraft Forum*, 2014.

[20] Chaumette F and Hutchinson S. Visual Servo Control, Part II: Advanced Approaches. *IEEE Robotics & Automation Magazine*, Vol. 14(1), 109-108, 2007.

[21] Hoencamp A. *Helicopter-Ship Qualification Testing*, PhD' s Thesis, Technische Universiteit Delft, 2015.

[22] *"The Beaufort Scale"*, MetOffice, 2010. [Online]. Available:http://www.metoffice.gov.uk/media/pdf/b/7/Fact_sheet_No._6.pdf. [Accessed: 20- Jun- 2016]

APPENDIX A – ADDITIONNAL INFORMATION
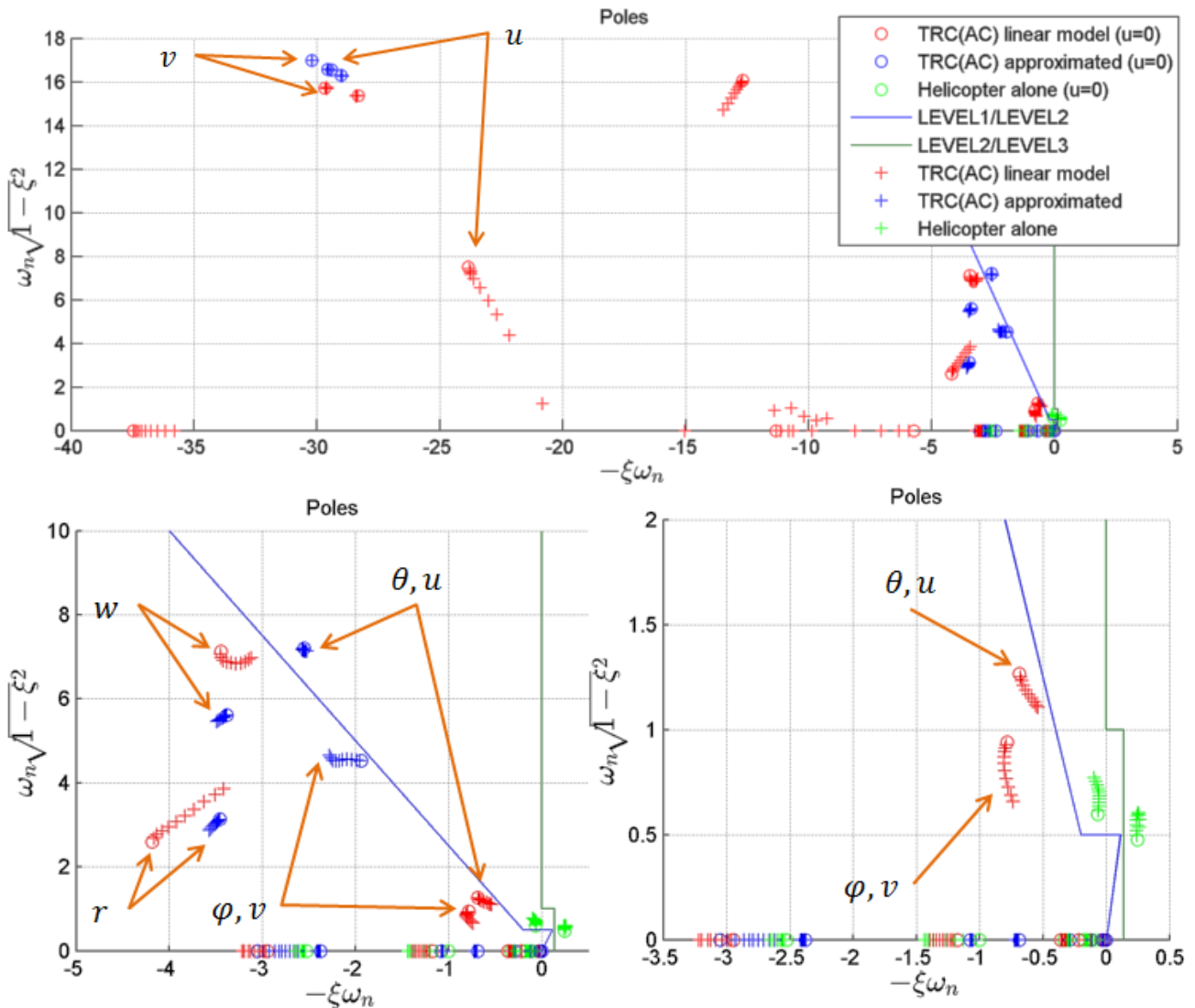
Figure 10 – Poles and identified Eigen modes, for speeds from 0 to 25 kt.

APPENDIX B – DEFINITION OF A SEA STATE 4

The initial data used to model a sea state 4 (moderate sea) is given in the Table below.

DOF	Displacement		Rate (deg/s or ft/s)	
	RMS	**Max/Min**	**RMS**	**Max/Min**
Roll	0.94°	3.5° / -4.1°	0.66 °/s	3.3 / -2.8
Pitch	0.91°	3.7° / -3.4°	0.89 °/s	3.9 / -3.3
Yaw	0.21°	1.2° / -0.7°	0.15 °/s	0.49 / -0.58
Sway	2.1 ft.	4.3 / -13 ft.	0.88 ft/s	3.3 / -3.7
Heave	2.5 ft.	25 / -3.5 ft.	2.4 ft/s	11.7 / -10.8

Table 6. Ship motion properties, as presented in [6]

This heave amplitude is not used here. Instead this paper uses the amplitude given by the Douglas sea scale for a state 4. Pulsation ω is deduced by assuming that for each DOF: $\omega = \frac{Max_{rate} - Min_{rate}}{Max_{displacement} - Min_{displacement}}$

The wavelength λ is taken from the Douglas Sea scale, mode details can be found in [22].

APPENDIX C – SIMULATION RESULTS

In this section N = 10 simulations were executed. For each simulation the initial helicopter pose is behind the ship, at a different point.
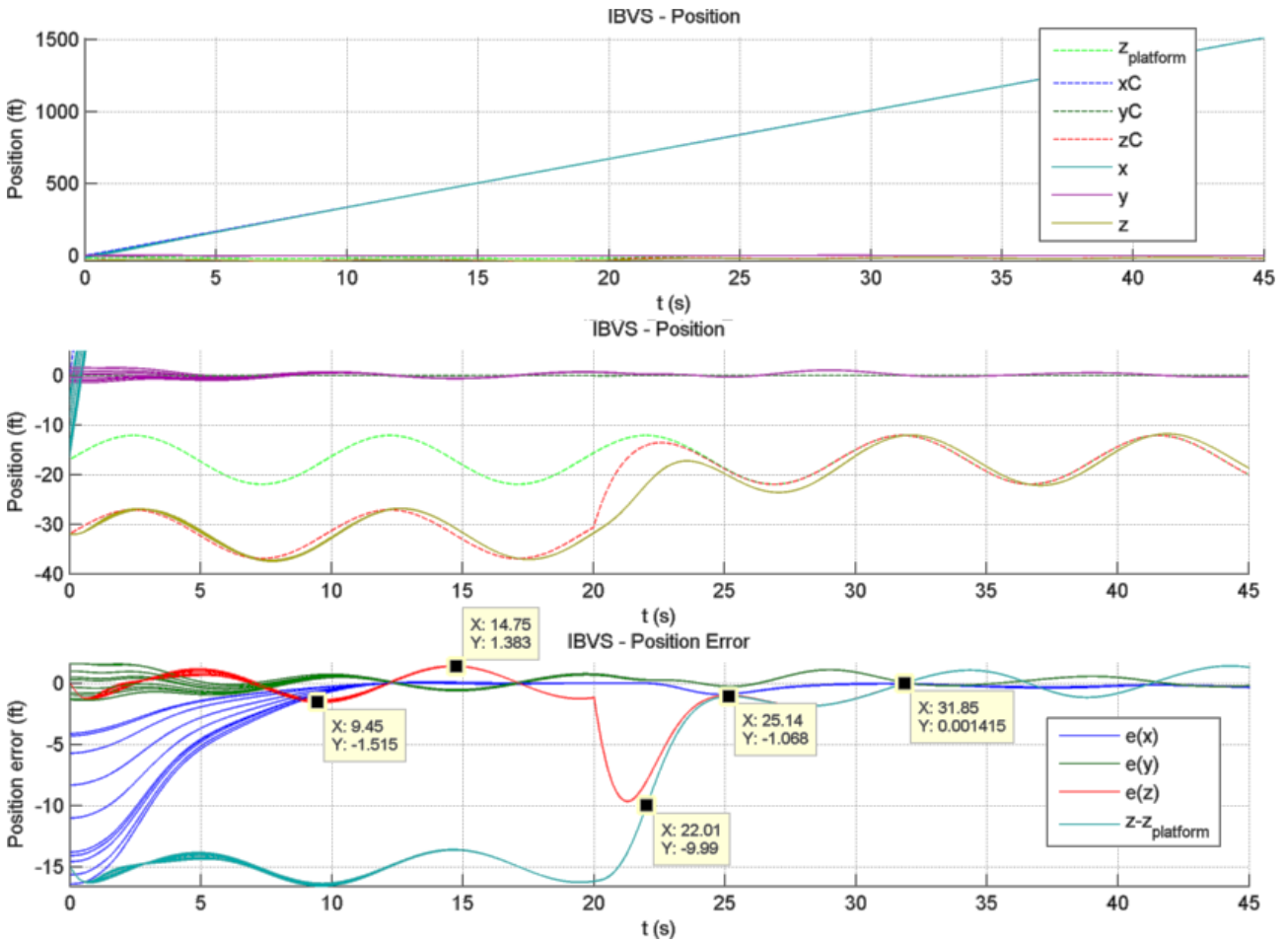
Figure 11 – Position tracking performances (Hover then landing)
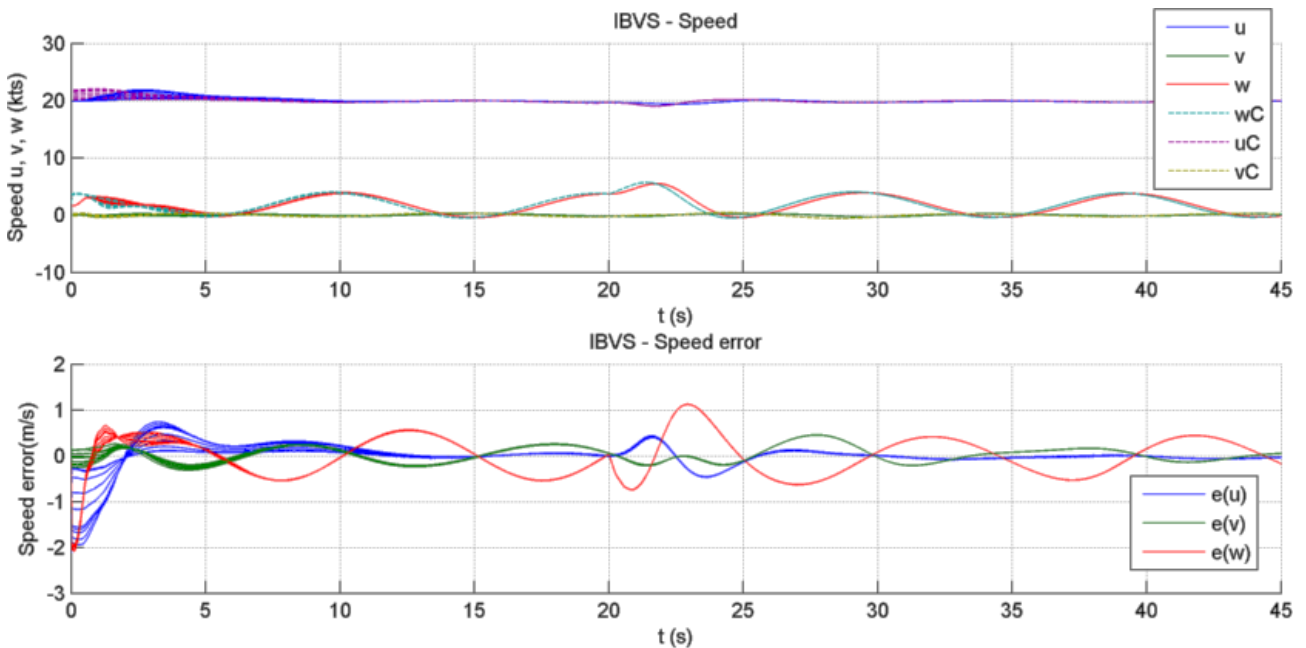
Figure 12 – Speed performances
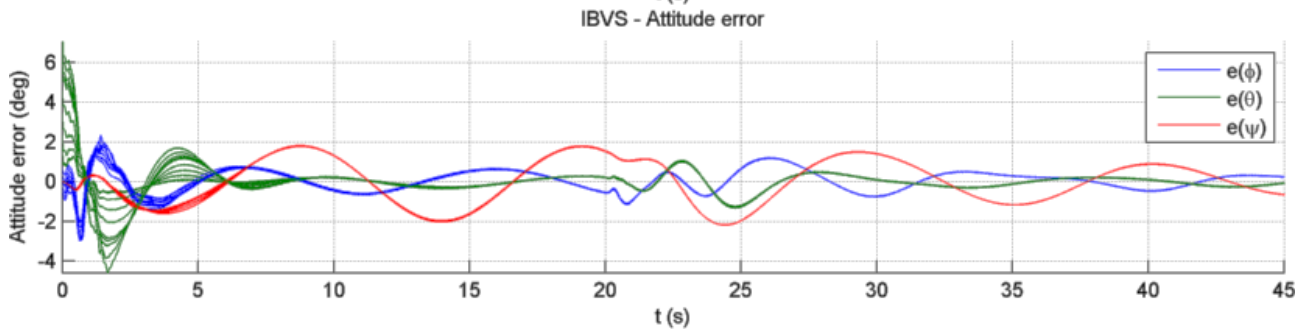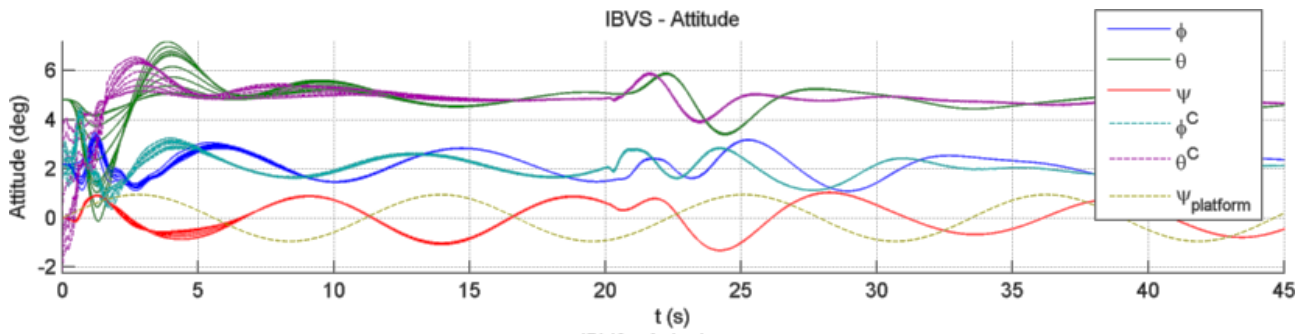
Figure 13 – Attitude performances
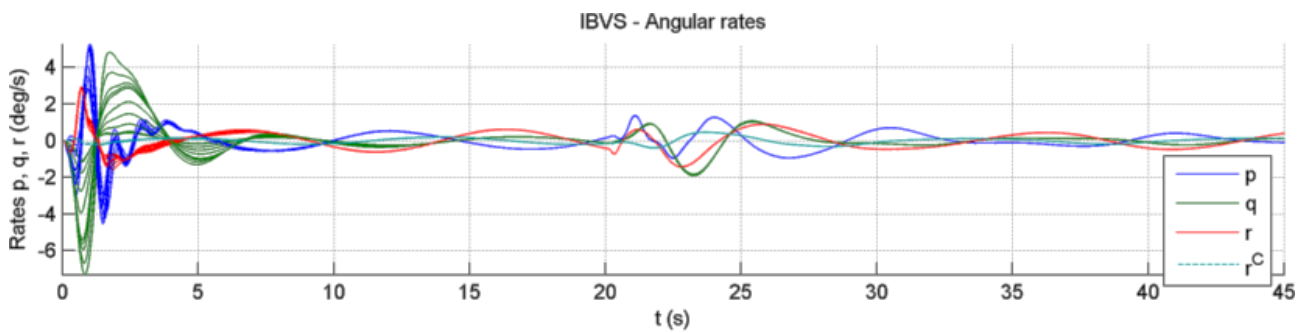
Figure 14 – Angular rates performances
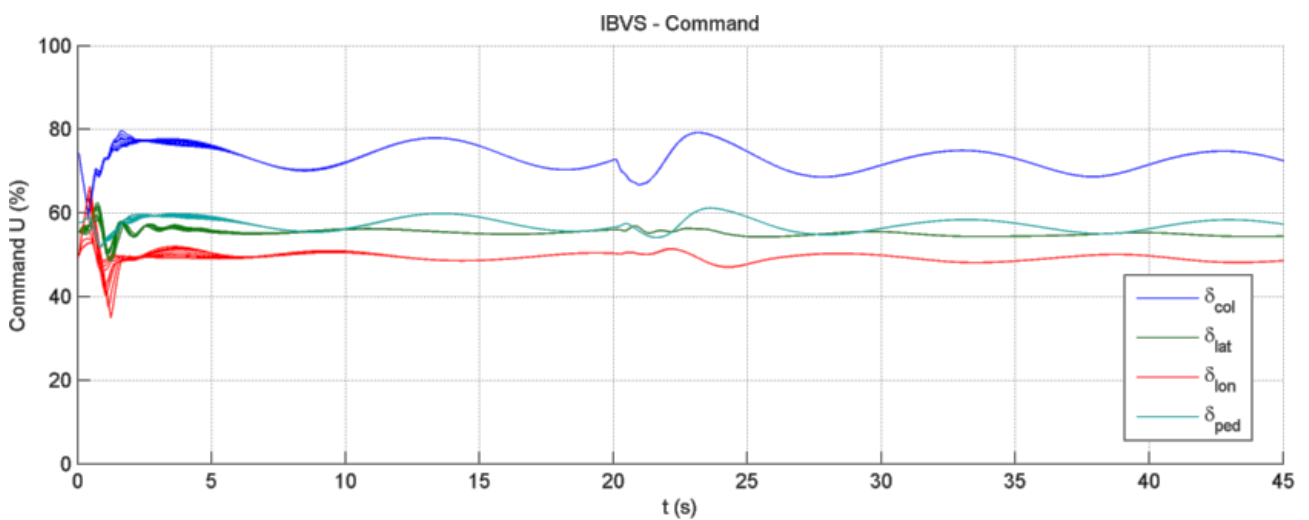
Figure 15 – Actual commands for actuators